Bistability and Transitions between Stable Operation and Thermo-Acoustic Instability in a Staged Liquid-Fuel Combustor

Antoine Renaud, Sebastien Ducruix, Laurent Zimmer

日本燃焼学会誌　第 59 巻 187 号（2017 年）33-40

Journal of the Combustion Society of Japan
Vol.59 No.187 (2017) 33-40

■特集／FEATURE■

―燃焼振動の基礎的研究／Fundamental Study of Combustion Oscillations ―

Bistability and Transitions between Stable Operation and Thermo-Acoustic Instability in a Staged Liquid-Fuel Combustor

RENAUD, Antoine[1,2]*, DUCRUIX, Sebastien[3], and ZIMMER, Laurent[3]

[1] *Aeronautical Technology Directorate, Japan Aerospace Exploration Agency, 7-44-1 Jindaiji-higashi Chofu, Tokyo 182-8522*

[2] *Faculty of Science and Technology, Keio University, Yagami campus, 3-14-1 Hiyoshi, Kohoku-ku, Yokohama, Kanagawa 223-8522*

[3] *Laboratoire EM2C, Universite Paris-Saclay, CentraleSupelec, Grande Voie des Vignes, 92290 Chatenay-Malabry, France*

Abstract : Because of increasingly stringent regulations on jet engines pollutant emissions, new ways of reducing them are needed. A promising way is the use of Lean Premixed Prevaporized (LPP) combustion where the liquid fuel is vaporized and mixed with air in excess before burning. In the present work, a model gas turbine combustor fed with liquid dodecane is studied experimentally. It is equipped with two fuel injection stages: a pressurized nozzle called the pilot and a multipoint device. When the split of the fuel injection between the stages is changed, several phenomena can be observed. The flame shapes can change drastically and present different behaviors, some of them showing a strong acoustic activity. In particular, two different flame shapes can be obtained for the exact same operating conditions depending on the burner history. The first flame, named *sV*, is stabilized thanks to an internal reaction zone that modifies the air flow compared to non-reacting conditions. The second state, associated with a *Lifted* flame, exhibits a strong thermo-acoustic instability linked to the quarter-wave mode of the chamber. A switch from the *sV* to the *Lifted* state can be triggered by air flow rate modulations while the opposite change can occur naturally as the fuel split is changed. These complex phenomena originate from multiple interactions between the fuel spray, the gaseous flow and the flame itself.

Key Words : Combustion, Flashback, PVC, Staging control

1. Introduction

Global air passenger traffic grows steadily by over 7% a year [1] and its environmental impact is a growing concern. In the recent years, increasingly stringent regulations of pollutant emissions have been imposed to engine manufacturers [1]. Traditionally used diffusion flames cannot provide enough potential for pollutant reduction anymore, especially regarding nitrogen oxides (NOx). This explains the need for a paradigm shift in the fuel combustion approach.

A promising lead to follow is lean premixed combustion where a good mixing between air in excess and fuel can help in reducing high temperature regions and thus thermal-NOx creation [2]. Some drawbacks however have to be overcome. Since jet fuel is liquid, a particular attention has to be given to the atomization, mixing and vaporization processes. Using a multipoint injection where fuel is finely atomized over a large region of the injector can help in creating an adequate premix between fuel and air. Nevertheless, lean premixed flames are prone to stability issues such as blow-off or thermo-acoustic instabilities [3,4]. The latter happen when heat release fluctuations from the flame couple with the acoustic resonance of the setup. The high amplitude pressure fluctuations that arise can have detrimental consequences, ranging from a reduction in engine performance to the complete destruction of the system [5]. To improve the stability of these flames, a pilot injection can be used. The idea is to inject a small quantity of fuel upstream of the main flame to create a region filled with hot burnt gases to permanently reignite the flame and stabilize it.

All this added complexity has an impact on the flame dynamics and the behavior of staged injectors remain to be fully understood. Indeed, numerical simulations [6] and experimental studies [7] tend to show that the flame shape and dynamics can strongly depend on the burner history or on external perturbations. In the present study, carried out at EM2C laboratory in CentraleSupelec in France, we analyze a particular operating point of a liquid fuel staged burner showing bistability between quiet operation and thermo-acoustic instability. The data

* Corresponding author. E-mail: antoine@arenaud.fr

comes from two Proceedings of the Combustion Institute articles [8,9] and a PhD thesis freely available online [10]. Steady flame stabilization mechanisms are described and transitions to and from thermo-acoustic instability are analyzed thanks to time-resolved measurements.

2. Experimental Methods

2.1. Experimental setup

The BIMER experimental device [8-10] used in this study is based on a simplified model of an industrial fuel injector developed by Snecma (now Safran Aircraft Engines). This injector is placed in a plenum upstream of the 500 mm-long combustion chamber which has a square section (150 mm) and silica windows for optical access. Its water-cooling allows for prolonged burner operation and steady boundary conditions. Because of its physical properties close to kerosene, dodecane is chosen as fuel and air flows through an electric preheater before entering the plenum in order to enhance vaporization and get closer to the compressor outlet temperature in a real engine. A horizontal cut of the injector and the beginning of the chamber can be seen in Fig. 1.

Each of the two stages of the injector consists in one air swirler and a fuel injection device. The swirlers are co-rotating and the geometrical design of the injector divides the air flow (controlled by a Bronkhorst In-Flow flowmeter) between the two stages. The upstream stage (light gray in Fig. 1) is called the pilot stage and has 13.5% of the air mass flow rate flowing through its 18-vane radial swirler (geometrical swirl number around 0.6). The fuel is injected from a pressurized nozzle (MMP 6390-0-0-03) creating a hollow cone of droplets. Downstream of the pilot stage is the take-off stage, shown in dark gray in Fig. 1. The remaining 86.5% of the air flow rate goes through its 20-vane radial swirler (geometrical swirl number around 1). A special characteristic of this stage is its fuel injection system called multipoint. Fuel is injected through ten 0.3 mm holes placed in cross flow with the air exiting the swirler in order to provide a fast atomization and mixing.

A key parameter regarding this injector's operating point is how much fuel is injected in each stage. This is monitor through the so-called staging parameter α, defined as:

$$\alpha = \frac{\dot{m}_p}{\dot{m}_p + \dot{m}_{TO}}$$

where $\dot{m}_p$ is the pilot fuel mass flow rate and $\dot{m}_{TO}$ is the take-off fuel mass flow rate. This parameter is thus the proportion of fuel injected in the chamber through the pilot stage. Since the multipoint injector provides a better atomization and mixing than the pilot pressurized nozzle, low values of the staging parameter are sought after.

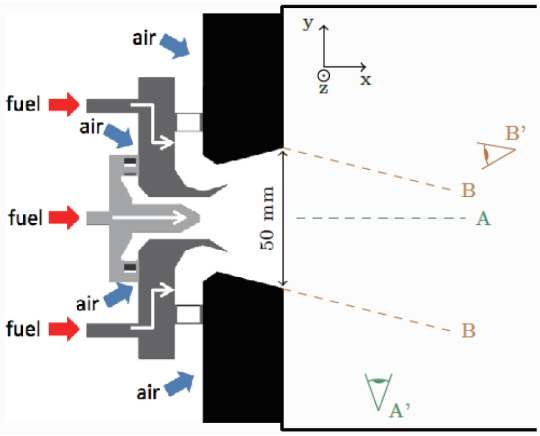

Fig. 1 Top view of the injection device positioned at the entrance of the combustion chamber, showing the two injection stages (pilot: light gray, take-off: dark gray). A laser sheet (A) illuminates the (x,z) plane in the center of the chamber to allow the observation (A') of the fuel droplets Mie scattering signal. An expanded laser beam (B) is sent in the injector hole to visualize (B') the fuel spray near the pilot fuel nozzle. From [9].

The test rig is also equipped with a siren-like device (CBOne, Graz, Austria) placed before the plenum to perform controlled air flow rate modulations. It works by rotating a toothed wheel in front of a nozzle through which the air flows. The rotational speed of the wheel controls the modulation frequency. The amplitude of the fluctuations is independently modified by changing the relative positions of the wheel and the nozzle. A thorough description of the system can be found in Giuliani *et al.* [11].

The chosen operating for the setup corresponds to an air flow rate of 43 g/s (preheated at 433 K) and a global equivalence ratio of 0.6, giving a thermal power around 72 kW. The staging parameter α is changed between 30% and 0% while the power is kept constant, giving rise to the studied phenomena.

2.2. Diagnostics

The fuel spray inside the chamber is observed through the Mie scattering signal of the droplets crossing a laser sheet. The associated setup is schematically shown as (A-A') in Fig. 1. A 1 mm thick light sheet is generated by two Nd:YAG lasers working at 10 kHz each with a delay of 20 μs between them. A high-speed camera (Photron Fastcam SA-5) equipped with a 50 mm, f:1.4 lens (Nikon) and a 532/10 nm bandpass filter records the light scattered by the droplets. The 704×520 pixels sensor records a 176×130 mm region. Particle Image Velocimetry (PIV) processing on two consecutive fuel spray images is performed. Because the Mie scattering signal from the droplets is used, the seeding is highly non-uniform and it must be kept in mind that the resulting velocity field may not necessarily represent the underlying air flow. The images are treated with the open source

PIVLab software, using a direct cross-correlation algorithm on 20×20 pixels (5×5 mm) interrogation windows with 60% overlap.

Because what happens inside the injector upstream of the combustion chamber can provide interesting information, a visualization technique aiming at observing the spray near the pilot nozzle is also used here, schematically represented as (B-B') in Fig. 1. It consists in sending an expanded laser beam (Nd:YAG, 10 kHz) into the hole linking the chamber and the injector and recording the Mie scattering signal from the early pilot fuel spray with a high-speed camera (Photron Fastcam SA-5) equipped with a 105 mm, f:5.6 lens (Nikon) and a 532/10 nm filter. Quantitative spatial information cannot be extracted from such images since light is send as an expanded beam but the high speed data allow for the temporal resolution of some phenomena.

To observe the flame shape and motions in the reacting cases, CH* spontaneous emission is recorded with a high speed camera (Photron Fastcam SA-X) equipped with a light intensifier (Hamamatsu C10880-03C), a 50 mm f:1.4 lens and a 431/10 nm bandpass filter. The 512×512 pixels images enable the recording of a 153×153 mm region in the beginning of the chamber. The orientation of the camera is the same as A' in Fig. 1 and the acquisition frequency is 10 kHz.

For all cases, the pressure fluctuations in the chamber are recorded with a B&K microphone (4938) placed in a home-built water-cooled semi-infinite waveguide located at half the length of the chamber. Its signal, as well as all synchronizing signals from the cameras, is acquired with a NI acquisition card (PCI-MIO-16E-4) at a 32768 Hz frequency.

3. Steady operation

3.1. Non-reacting case

Before analyzing the behavior of the burner in reacting conditions, a non-reacting study of the spray and flow field is first carried out and results are shown in Fig. 2. The staging parameter is fixed at 15% and air is still preheated at 433 K but no combustion takes place. Fuel spray contours are obtained from the Mie scattering recordings inside the combustion chamber. Because the signal is created by relatively dilute small droplets, what matters is the fluctuations of the pixel values over the recording length rather than their average intensity which would only highlight background features. The contours shown in Fig. 2 (and later in Fig. 4) are thus based on the Root Mean Square (RMS) image created with the RMS value for each individual pixel. The black line follows a threshold set at 15% of the maximum RMS value and shows that the fuel spray is mostly spread out, seemingly indicating a good mixing between fuel and air. PDA measurements performed for this operating point

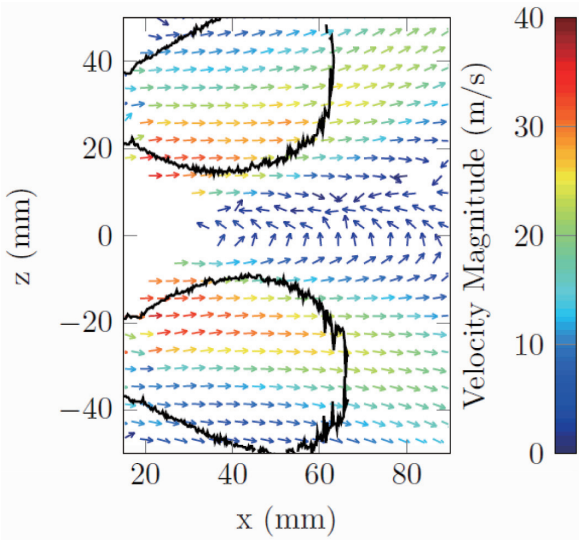

Fig. 2 Average spray velocity direction (arrows) and magnitude (color) in non-reacting conditions. The black contour line corresponds to the spray limits defined by a thresholding of the Mie scattering RMS image. From [9].

allowed to compute size-conditioned velocity fields, showing that the majority of the droplets in the spray have a relatively low Stokes number and are thus good tracers of the air flow [10]. The PIV treatment of the Mie scattering images can thus provide information on the gaseous flow.

In the average velocity field for the non-reacting case shown in Fig. 2, it can be seen that most of the flow goes towards increasing axial coordinates with velocities between 15 and 35 m/s. It is also diverging but on average less than 15^0 from the horizontal. A recirculation zone where the flow direction is reversed with velocities below 10 m/s can also clearly be identified near the axis. These features are typical of a swirling flow with a vortex breakdown in a confined environment, which creates a swirling jet and Inner and Outer Recirculation Zones (IRZ and ORZ). Here, the use of PIV on fuel droplets in a preheated environment prevents from obtaining data from the ORZ (out of the field of view of Fig. 2) and the upstream part of the IRZ. Indeed, only the smallest droplets can enter into these regions and they vaporize before contributing to give valid velocity values.

From a dynamical point of view, analyses of the chamber Mie scattering fields show the presence of a coherent structure that creates a helical-like modulation inside the spray. Studies of this phenomenon [7] have shown that it corresponds to the trace of a Precessing Vortex Core (PVC, [12]) that has roots near the pilot nozzle. In order to monitor the PVC at its origin, internal Mie scattering visualizations are used (B-B' in Fig. 1). They show that the spray cone generated by the pilot nozzle presents a precessing motion which is then responsible for the helical-like modulation observed in the spray once in the chamber [10]. Thanks to a

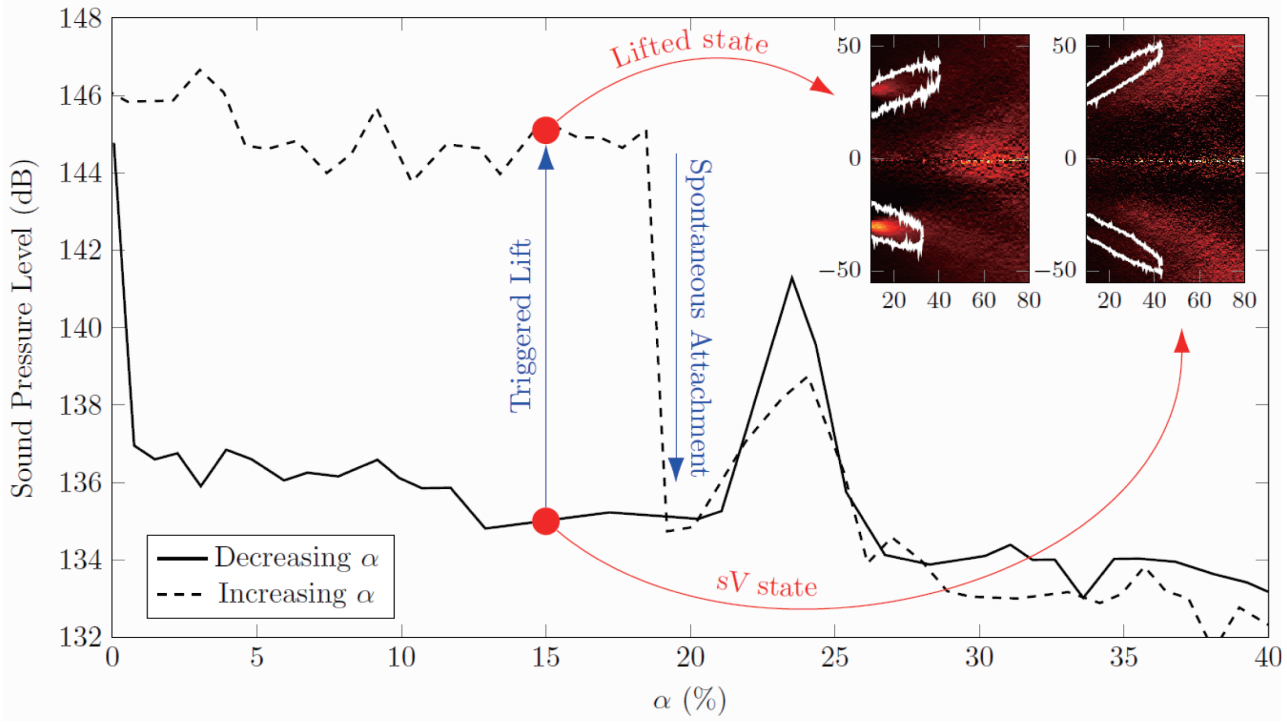

Fig. 3 Sound Pressure Level in the chamber as a function of the fuel staging parameter. Only the fuel repartition is changed, all the other controlling parameters are kept constant. Abel-inverted mean chemiluminescence images are added for the two studied steady states.

small averaging window in the image, it is thus possible to obtain a signal that contains the precession frequency of the structure. Continuous wavelet transform [13] is then used to analyze the signal with a complex Morlet wavelet at scales chosen to provide a 2 Hz resolution in the 1900-2100 Hz band. In the present non-reacting case, the PVC average frequency is measured at 1951 Hz (standard deviation: 14 Hz).

3.2. Hysteresis cycle

The burner is now operated in reacting conditions. After ignition at a low power, the operating point is reached and the air and fuel flow rates are then kept constant. The fuel repartition between the pilot and take-off stages is slowly changed so that the staging parameter α varies between 0% and 40%. The pressure fluctuations in the chamber are monitored as α is decreased from 40% to 0% and then increased back to 40%. The plot of the Sound Pressure Level (SPL) versus the staging parameter during this operation can be seen in Fig. 3.

Starting from 40%, decreasing the fuel staging leads to a moderate sound pressure level in the chamber until α reaches a region between 20 and 26% where higher values are encountered. This region being out of the focus of the present study, further information will not be explicitly provided but can be found in [10]. After this peak, the sound pressure level retains the previous values until a staging of almost 0% is reached, meaning that all the fuel is injected through the multipoint injector. At this point, a sudden increase of about 10 dB can be witnessed, highlighting a drastic change in the burner behavior. A side note must however be made on the validity of this 0% staging. Indeed, around this point the precision of the pilot fuel flow meter becomes poor and staging parameter values below 5% must thus be treated with care. As α start to increase back from 0%, the sound pressure level remains high. This corresponds to a clear hysteretic behavior, leading to two different burner responses for the exact same operating point. As the staging parameter keeps increasing, another sudden change is encountered a bit before 20% where the sound pressure level quickly drops to smaller values corresponding to the range obtained while decreasing α. Finally, further increases in the pilot fuel proportion lead to a path very similar to the one taken in the opposite direction.

From a real engine point of view, the operating point of choice would be among these low values of the staging parameter since the multipoint injection is here to improve fuel mixing and thus reduce the pollutant emissions. Not being able to know the burner behavior is thus a strong drawback, especially when one of the states shows such a strong noise production because of a thermo-acoustic instability.

The Abel-inverted mean CH* chemiluminescence images shown in Fig. 3 indicate that the two branches of the hysteresis cycle are associated with two different flame shapes. This bistability of the burner is studied in the following section.

3.3. Bistable states

As the staging parameter is kept constant at 15%, the spray and flame shapes and behaviors are studied for the two stable points that can be reached, one from decreasing α and the other from increasing it.

First, the state associated with the lowest SPL (around 135 DB, when α is decreasing) is studied. According to the mean chemiluminescence images in Fig. 3, the reaction zone is not strongly marked and is globally diverging away from the chamber axis. At the top border of the image, it seems to progress slightly upstream, thus showing an interaction with the chamber walls. It thus looks like a classical V-shaped flame but in a more "diluted" fashion. During the rest of the study, this state is referred to as the *sV* state. Looking at the flame position relatively to the spray (white contour), it seems that reaction happens mostly towards the inner part of the liquid fuel droplets cone. The shape of the latter seems different from what is observed in non-reacting conditions (black contour in Fig. 2), being much thinner and diverging, even though its external borders seem similar. The mean velocity field in Fig. 4 (top) shows a strong change in the flow compared to the non-reacting conditions. A visibly diverging behaviour (close to 30^0 from the horizontal) can indeed be observed with a uniform velocity magnitude (above 55 m/s) in the spray region. The PVC is still present and a wavelet transform performed similarly to the non-reacting case shows that its frequency has increased to 2017 Hz and its frequency fluctuations have decreased (standard deviation: 6 Hz). This change indicates that, in this case, the air flow inside the injector has changed from the non-reacting case. This is likely to be the effect of an internal pilot flame anchored inside the injector [10]. It is interesting to note that, as it combines a low value of α (meaning an expected good premixing) with only moderate pressure fluctuations, the *sV* state seems a good proof that staged multipoint injectors have the capability to reach pollutant emission reduction targets and prevent thermo-acoustic instabilities.

When α is increasing, Fig. 3 shows that the SPL is high, around 145 dB. The associated reaction zone seems mostly spread in the downstream part of the region of interest with signal around the axis of the chamber, probably because of turbulent motions. Some signal can also be observed upstream but it does not originate from the inside of the injector and is highly intermittent. This leads to believe that the flame is completely detached and thus aerodynamically stabilized by the swirling flow. The name used to refer to this state is thus *Lifted* state in the rest of the paper. The spray (in white in Fig. 3 and also in black in Fig. 4) looks thicker than in the *sV* state. The average velocity field, shown on the bottom half of Fig. 4, presents velocity magnitudes between 20 and 45 m/s while the flow is not strongly diverging (around 20^0 from the horizontal).

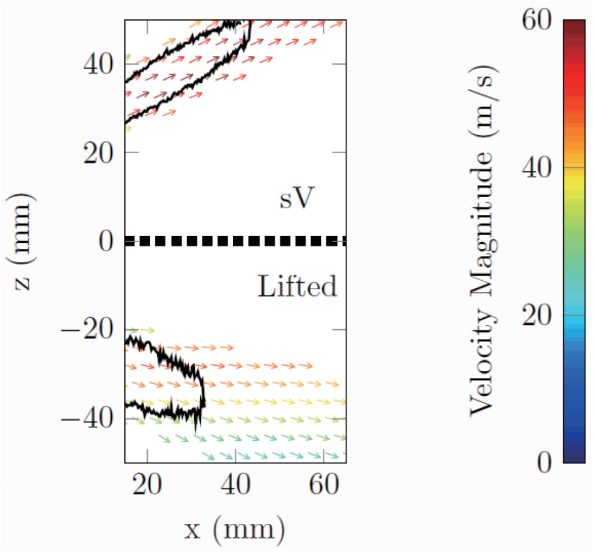

Fig. 4 Average spray velocity direction (arrows) and magnitude (color) in reacting conditions for the *sV* (top) and lifted (bottom) states. The black lines represent the average spray shape in each case. From [9].

This brings the flow in the lifted state closer to the non-reacting case than to the *sV* state. The increase in velocity is likely to come from the density decrease due to the flame heat release but no strong change in the flow topology is witnessed. From a dynamical point of view, the internal visualizations show that the PVC is still present, although less marked than for the *sV* flame. The average precessing frequency in the present case is 1967 Hz (standard deviation: 13 Hz) which is interestingly similar to the non-reacting case. From all these observations, the lifted flame thus seems to correspond to a premixed-like flame stabilization inside the chamber with a weak feedback of the flame on the mean flow. The most interesting feature of this flame is however the high amplitude pressure fluctuations associated with it. They correspond to a strong thermo-acoustic instability around 330 Hz, which is related to the quarter-wave mode of the chamber. This instability is responsible for the overlap of the flame and spray signals in the upstream region (X<30 mm) of the mean *Lifted* flame image in Fig. 3. A precise study of this region [9] has shown that there is actually an alternation of liquid fuel and flame but that the two do not coexist at the same point. The delay between the two signals is likely to come from the droplet vaporization time which is identified as a main contributor to the instability feedback mechanism.

4. Transient phenomena

In the present section, ways of switching from one state to the other are presented, corresponding to the vertical arrows in Fig. 3. First, with the help of air flow rate modulations, the switch

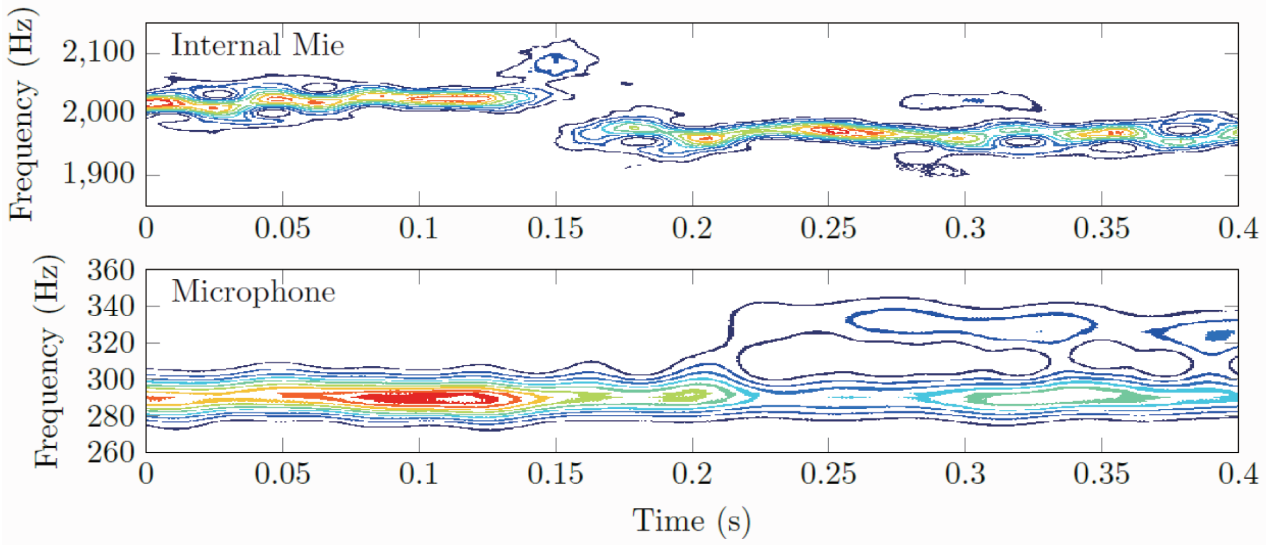

Fig. 5 Scalograms of two signals during the siren-induced lift of the flame. Top: internal Mie scattering signal around the PVC frequency. Bottom: microphone signal around the thermo-acoustic instability frequency. The contours represent levels corresponding to multiples of 10% of the maximum. From [9].

from the *sV* state to the *Lifted* state is studied and then the natural switch back to the *sV* state is analyzed.

4.1. Triggered lift

To trigger the lift of the flame, the siren is operated at a fixed frequency of 290 Hz and the amplitude of the modulations is slowly increased while the burner operating point is kept stable at α=15%. Even though it seems to be a frequency of interest, forcing at 330 Hz would prevent the detection of the onset of the thermo-acoustic instability as it would be covered by the siren effect. The 290 Hz value is also chosen to enable comparison with studies already performed at different operating points [10] but similar results have been obtained with other excitation frequencies. In order to study the triggered lift of the flame, the time-frequency content of two signals is analyzed using scalograms from continuous wavelet transform, shown in Fig. 5. The first signal comes from the internal Mie scattering visualization and responds well to the PVC. It was already used in the previous sections and enables to detect the switch between the two states from the internal aerodynamical point of view. The second signal comes from the microphone and enables to detect the onset of the 330 Hz thermo-acoustic instability that characterizes the *Lifted* state. Since we are interested here in the temporal detection of the lift, the bandwidth parameter of the wavelets is chosen so that they give the same 0.02 s precision at 2000 Hz for the internal Mie scalogram and at 310 Hz for the microphone one. At the beginning of the recording, it can be seen that the PVC frequency, as detected by the internal Mie scattering signal, is above 2000 Hz while it is between 1950 and 2000 Hz at the end. The transition from the *sV* state to the *Lifted* state from the air flow point of view can clearly be identified as the abrupt drop in frequency at 0.15 s. In the microphone signal scalogram, the trace of the siren modulation at 290 Hz can be observed throughout the recording duration. An additional structure around 330 Hz appears at the end, it is the thermo-acoustic instability associated with the *Lifted* state. Interestingly, the onset of this instability is after 0.2 s, that is more than 50 ms after the aerodynamical change. This shows that the thermos-acoustic instability is only a consequence of the lift of the flame and of the change of the flow structure. The mechanism between the switch can in fact be attributed to the blow off of the internal pilot flame by the siren-induced air flow modulations [14]. This prevents the flame to anchor and stabilize in the *sV* state and renders it more sensitive to potential thermo-acoustic instabilities. It must be noted that the flame remains in the *Lifted* state even when the siren is stopped after the switch, leading to the hysteresis phenomenon observed in Fig. 3.

4.2. Natural re-attachment

After the lift of the flame, whether naturally through really low values of α or forced by the siren, it is necessary to increase the staging parameter to bring back the flame to the *sV* state. This natural transition is a very complex event, thoroughly studied in [10], that can happen for different values of the staging parameter depending on small variations of the control parameters. For the present operating point, it occurs between roughly 17% and 21%. It consists mainly of two steps: first the flame that was in the *Lifted* state anchors inside the injector with a new shape called *Tulip* and then this new shape widens to give a *sV* flame. Only the first step is studied here as the second one remains to be fully

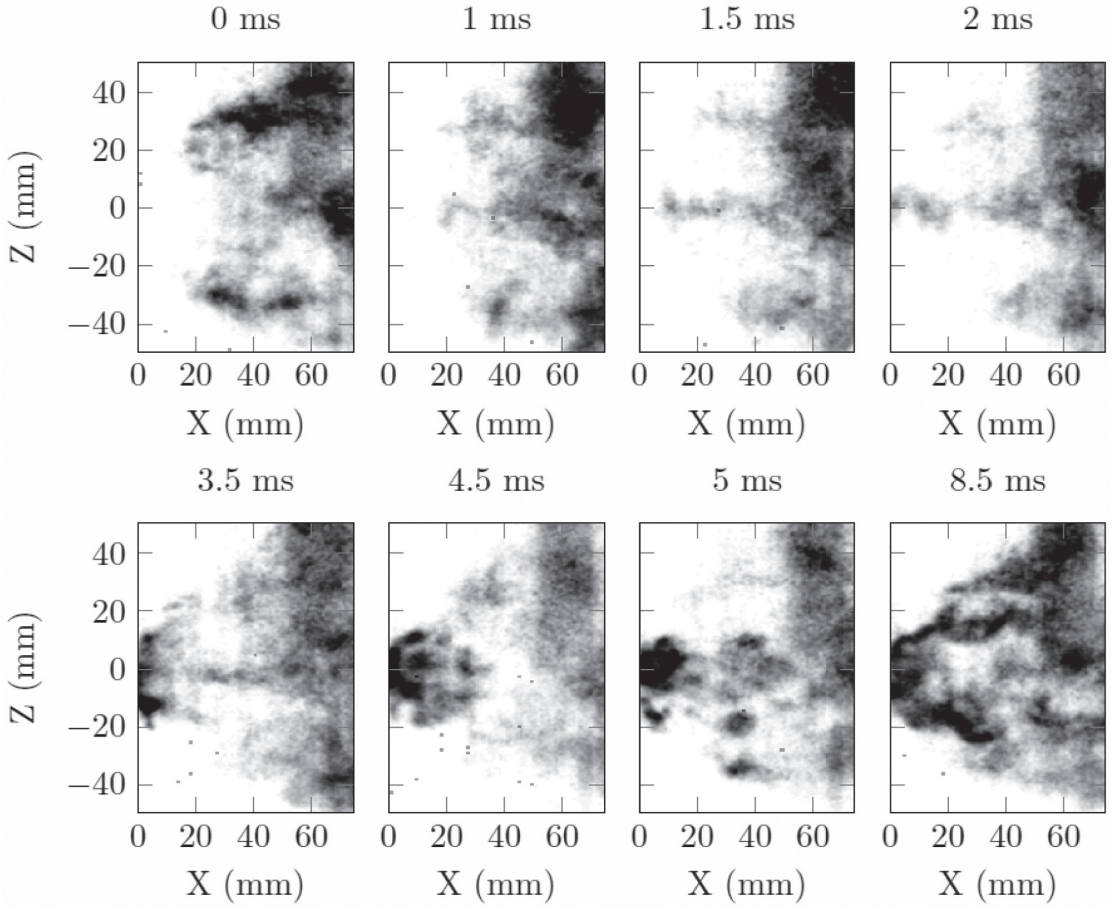

Fig. 6 Instantaneous CH* chemiluminescence images at different instants during the attachment step of the transition.

understood, even though some explanations are advanced in [10].

For the study of the re-attachment of the flame, high-speed chemiluminescence data are used since the phenomenon happens in less than 10 ms. For visualization purposes, the instantaneous chemiluminescence images presented in Fig. 6 are inverted meaning that black corresponds to high intensities and white to no signal with shades of gray in between. Time stamps with an arbitrary origin are added in the images to monitor the duration of the phenomena. The first image is clearly related to the lifted flame with no reaction occurring in the beginning of the chamber and most of the combustion located after X=60 mm. The last image corresponds to an instantaneous snapshot of the newly introduced *Tulip* state. The top row of Fig. 6 corresponds to the propagation of the flame from the main reaction zone to the injector. Indeed, in the center of the chamber for images 2 to 4, a finger-like structure moving upstream can be observed. This corresponds to a flashback, happening inside the IRZ because of the reverse axial velocity. After this flashback step, the flame has reached the inside of the injector. Then, nothing seems to happen for about 1 ms and the images look like the first one showing a lifted flame. During this period, things are however happening inside the injector, namely the internal flame ignition and anchoring. Interestingly this period can result in a failure of the transition and nothing happens until another flashback occurs. Key mechanisms are thus probably at stake inside the injector but are unfortunately hidden. Finally, if this hidden step is successful, what is seen is shown on the bottom row of Fig. 6. The flame appears from the inside of the injector in the beginning of the chamber as shown on the fifth image. It then propagates downstream, corresponding to the new possibility for the flame to consume the fuel spray from the inside of the cone. This motion ends up giving the expected *Tulip* flame and the flame is now attached.

This first step is thus strongly dependent on two phenomena: a flashback to bring the flame in the injector and the success of the ignition inside the injector. The first phenomenon is created by the increase in the pilot fuel flow rate as α increases which provides combustible mixture in the IRZ. The success of ignition inside the injector remains however very complex to study even though parameters influencing it have been identified [10].

5. Conclusions

In a staged aeroengine model combustor, a bistable behavior is

observed when most of the liquid fuel is injected through the multipoint stage. The occurrence of the states depends on the burner history as well as on potential external perturbations. The prediction of the combustor behavior is thus impossible if one only knows the operating parameters, which is a major deterrent for industrial application.

The philosophy of a staged multipoint injector is to provide the stabilization of a well premixed main flame thanks to burnt gases and heat from a lower power pilot flame. In the present study, this goal seems to be achieved when the combustion occurs in a *sV* state where an internal pilot flame helps in anchoring a broader reaction zone. The expected properties of such a flame with a good premixing and no thermo-acoustic instability also seem reached. When the pilot fuel flow rate reaches really low values or when air flow rate fluctuations occur however, the flame detaches and the sound pressure level in the chamber increases by 10 dB. This switch is associated with the extinction of the pilot reaction zone, enabling the main flame to move more freely. The resulting *Lifted* state is close to the non-reacting conditions from the mean air flow point of view but triggers a strong thermos-acoustic instability based on the quarter wave mode of the chamber. The feedback mechanism is based on a delay between flame and liquid fuel spray oscillations involving the vaporization time of the droplets. Obviously, such a state must absolutely be avoided in a real engine.

These complex phenomena come from multiple interactions between the flame, the liquid fuel and the air flow. They were furthermore observed under atmospheric pressure and with a simplified geometry and reduced power compared to realistic cases. Despite impressive advances in numerical simulations, such complex cases also remain a strong challenge for computations. Adding the increasing complexity of real aeroengines as a whole to the picture, it is obvious that the issues surrounding the reduction of pollutant emissions and the prevention of thermo-acoustic instabilities can only be tackled with combined efforts from experiments, simulations and theory.

Acknowledgments

The stay of A. Renaud at Jaxa and Keio University has been supported by the Erasmus Mundus EASED program (Grant 2012-5538/004-001) coordinated by CentraleSupelec.

References

1. International Civil Aviation Organization, *Annual Report of the ICAO Council* (2015).
2. Lefebvre, A. H., *Journal of Engineering for Gas Turbines and Power* 117: 617-654 (1995).
3. Candel, S., *Proc. Combust. Inst.* 29: 1-28 (2002).
4. Huang, Y., Yang, V., *Progress in Energy and Combustion Science* 35: 293-364 (2009).
5. Krebs, W., Flohr, P., Prade, B., Hoffmann S., *Combustion Science and Technology* 174: 99-128 (2002).
6. Hermeth, S., Staffelbach, G., Gicquel, L., Anisimov, V., Cirigliano, C., Poinsot, T., *Combustion and Flame* 161: 184-196 (2014).
7. Providakis, T., Zimmer, L., Scouflaire, P., Ducruix, S., *Journal of Engineering for Gas Turbines and Power* 134 (2012).
8. Renaud, A., Ducruix, S., Scouflaire, P., Zimmer, L., *Proceedings of the Combustion Institute* 35: 3365-3372 (2015).
9. Renaud, A., Ducruix, S., Zimmer, L., *Proc. Combust. Inst.* 36 (2016, In Press).
10. Renaud, A., *High-speed diagnostics for the study of flame stabilization and transient behavior in a swirled burner with variable liquid-fuel distribution,* PhD Thesis, Université Paris-Saclay, France (2015).
11. Giuliani, F., Lang, A., Gradl, K.J., Siebenhofer, P., Fritzer, J., *Journal of Engineering for Gas Turbines and Power* 134 (2012).
12. Syred, N., *Progress in Energy and Combustion Science* 32:93-161 (2006).
13. Grossmann, A., Kronland-Martinet, R., Morlet, J., in: *Wavelets*, Springer (1989).
14. Hardalupas, Y., Selbach, A., Whitelaw, J.H., in: *Laser Techniques Applied to Fluid Mechanics,* Springer (2000).